Design of two-dimensional photonic crystal defect states for quantum cascade laser resonators - Supplemental Data

Kartik Srinivasan§ and Oskar Painter†

† Thomas J. Watson, Sr. Laboratory of Applied Physics, California Institute of Technology, Pasadena, CA 91125, USA

Abstract. We present additional finite-difference time-domain (FDTD) simulations to supplement the data presented in the main text (http://www.arxiv.org/abs/physics/0410068).

PACS numbers: 42.70.Qs, 42.55.Sa, 42.60.Da, 42.55.Px

1. FDTD Simulations

1.1. Hexagonal Lattice

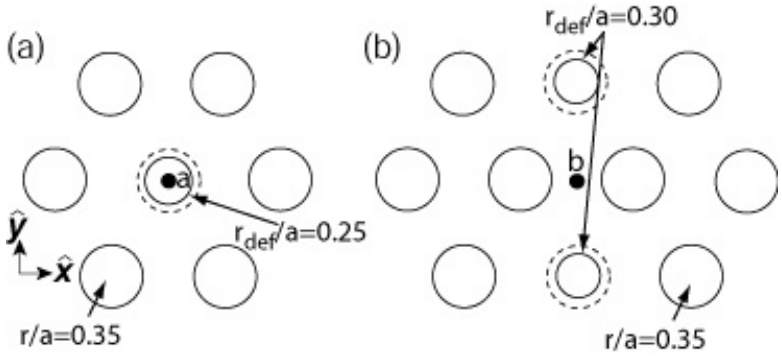

Figure 1. Defect geometries for donor modes about the (a) a-point and (b) b-point.

The main text considers a defect centered about point b as in Figure 1(b). Here, we choose our defect as a single reduced-size air hole centered about point a with $r/a = 0.35$ and $r_{def}/a = 0.25$ (Figure 1(a)). The spectrum for A_1 symmetry modes (FDTD-generated spectra represent an average of $E_z(\omega)$ taken over several spatial points in the lattice), given in Figure 2(a), shows a single dominant peak in the frequency range of interest ($a/\lambda_0 \approx 0.25 - 0.35$). The real space and Fourier space versions of this field are shown in Figure 2(b)-(c); we see that the mode has dominant Fourier components at

§ To whom correspondence should be addressed (kartik@caltech.edu)

the six J-points, as predicted in Table 2 (main text). Performing a similar analysis for the B_1 symmetry modes gives the Fourier transformed field shown in Figure 2(d), with dominant Fourier components again at the six J-points, consistent with the symmetry analysis predictions. The B_1 mode, however, is fairly delocalized in real space (evident from the localized peaks in Fourier space in Figure 2(d)), a result of the relatively weak confining potential the chosen defect creates for B_1 symmetry modes.

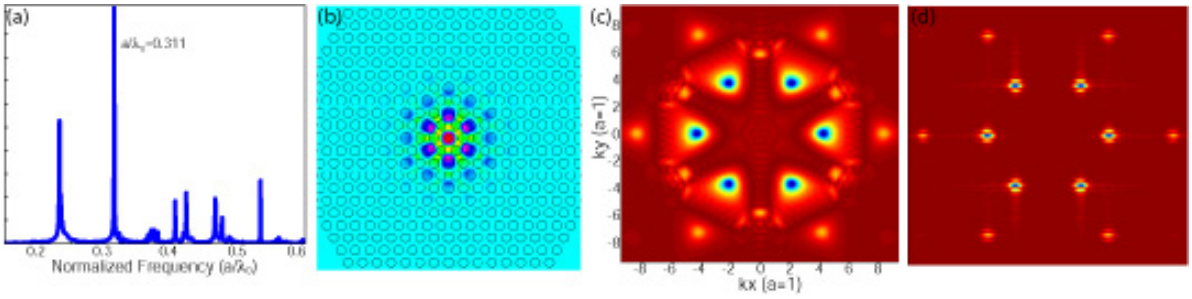

Figure 2. Donor modes about a-pt. in the hexagonal lattice. (a) Spectrum for A_1 symmetry modes. (b) $|\mathbf{E}|$ for A_1 mode. (c) $|\widetilde{\mathbf{E}}_z|$ for A_1 mode. (d) $|\widetilde{\mathbf{E}}_z|$ for B_1 mode. In (d) and from this point on, all 2D spatial Fourier transforms will be plotted over the domain $(k_x a, k_y a) = [-3\pi, -3\pi]..[3\pi, 3\pi]$.

1.2. Square Lattice

The main text considered defect modes centered about point f in the square lattice, formed by a defect such as that in Figure 3(c). Here, we consider defect states formed about points d and e.

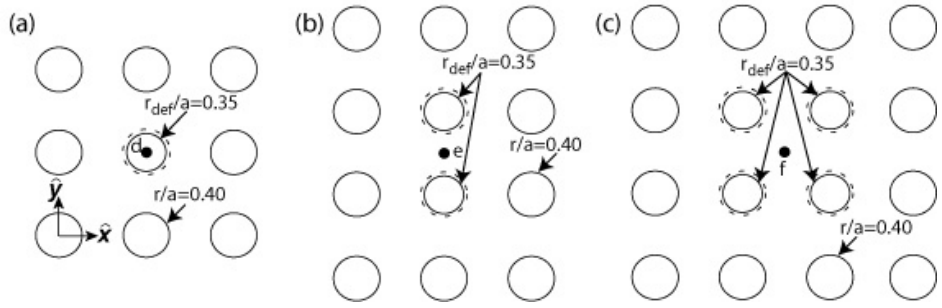

Figure 3. Defect geometries for donor modes about the (a) d-point and (b) e-point and (c) f-point.

To produce donor modes about the d-point, we consider a single reduced air hole with $r/a = 0.40$ and $r_{def}/a = 0.35$ (Figure 3(a)). From our group theory analysis, we expect two X-point donor modes, of symmetry A_1'' and B_2'' under C_{4v}. Under the reduced symmetry C_{2v}, both of these modes are of type A_1 symmetry. Similarly, the M-point donor mode is of type A_1'' symmetry under C_{4v} and type A_1 symmetry under

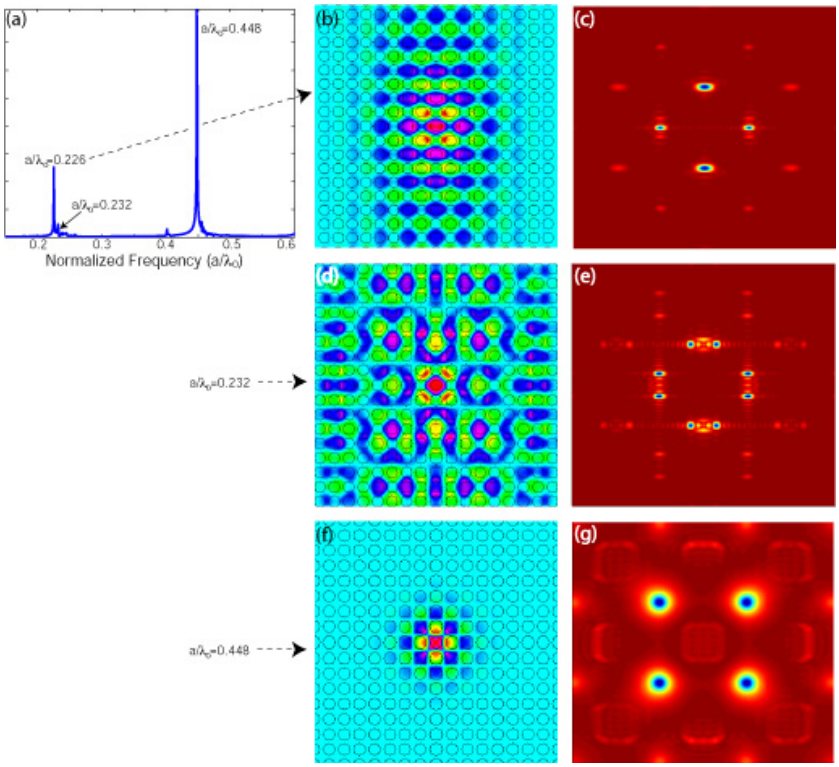

Figure 4. Properties of d-pt modes. (a) A_1 symmetry mode spectrum. (b) $|\mathbf{E}|$ for low freq. A_1 mode. (c) $|\widetilde{\mathbf{E}}_z|$ for low freq. A_1 mode. (d) $|\mathbf{E}|$ for mid freq. A_1 mode. (f) $|\widetilde{\mathbf{E}}_z|$ for mid freq. B_2 mode. (g) $|\mathbf{E}|$ for high freq. A_1 mode. (h) $|\widetilde{\mathbf{E}}_z|$ for high freq. A_1 mode.

C_{2v}. Examining the FDTD-generated spectrum for A_1 modes given in Figure 4(a), we in fact do see three primary peaks, a pair of which occur between $a/\lambda_0 = 0.20 - 0.25$, corresponding to the X-point donor modes, as well as a dominant peak at $a/\lambda_0 = 0.448$, corresponding to the M-point donor mode. Plotting the Fourier transformed electric fields for the two low frequency modes in Figure 4(c),(e), we see that the modes are in fact composed of the four X points in the IBZ, as predicted by the group theory analysis. The real space version (Figure 4(b)) of the lowest frequency mode shows it to be fairly well localized in real space, while the mode of slightly higher frequency (Figure 4(d)) is more delocalized. The real and Fourier space versions of the electric field of the high frequency peak are shown in Figure 4(f)-(g). The field is primarily composed of peaks at the four M points in the IBZ, as expected. As a result of the rather larger band-gap surrounding the M point of the fourth frequency band (main text, Figure 2(a)), this mode is well-localized in real space.

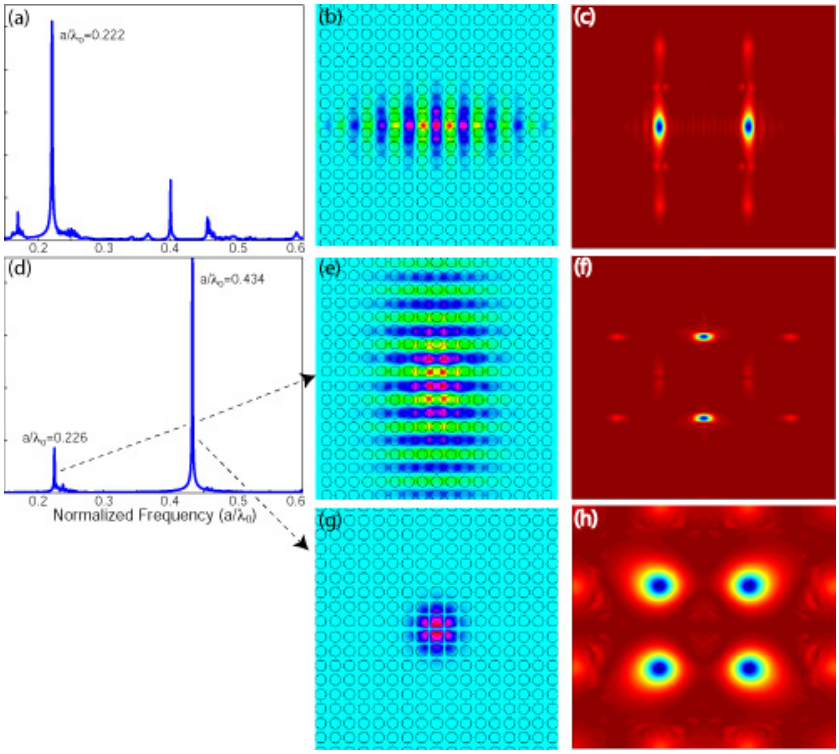

Figure 5. Properties of e-pt modes. (a) A_1 symmetry mode spectrum. (b) $|\mathbf{E}|$ for low freq. A_1 mode. (c) $|\widetilde{\mathbf{E}}_z|$ for low freq. A_1 mode. (d) B_2 symmetry mode spectrum. (e) $|\mathbf{E}|$ for low freq. B_2 mode. (f) $|\widetilde{\mathbf{E}}_z|$ for low freq. B_2 mode. (g) $|\mathbf{E}|$ for high freq. B_2 mode. (h) $|\widetilde{\mathbf{E}}_z|$ for high freq. B_2 mode.